Citation:
B. W. Stevens and M. F. Younis, "Geospatial Cognitive Networking Protocols and Sensing Algorithms for 5G NR Beamforming," in IEEE Transactions on Cognitive Communications and Networking, 2022, doi: 10.1109/TCCN.2022.3204536.

DOI:
https://doi.org/10.1109/TCCN.2022.3204536

Geospatial Cognitive Networking Protocols and Sensing Algorithms for 5G NR Beamforming

Brian W. Stevens and Mohamed F. Younis
The University of Maryland Baltimore County and Johns Hopkins University Applied Physics Laboratory
Email: brian.stevens@jhuapl.edu, younis@umbc.edu

***Abstract*— Although 5G New Radio (NR) has created new opportunities for cognitive radio networks, its increased physical layer security and flexibility limit the usefulness of traditional cognitive detectors such as energy and blind control channel algorithms. This paper presents CASINO-NR, a novel framework for establishing a cognitive self-reliant secondary network with no additional physical infrastructure, collaboration from the primary network nodes, and software or hardware changes to the existing 5G network. CASINO-NR includes a novel beam detection algorithm that finds and ranks 5G NR synchronization signals to determine geospatially non-interfering beams for secondary communications. We compare the developed beam detector with multiple existing approaches for sensitivity to interference and phase distortions. We also apply power control to prevent interference on neighboring beams. CASINO-NR is analyzed against the estimated throughput capacity and capabilities of other cognitive detectors found in literature. Finally, we examine an experimental beamforming example to demonstrate our beam detection algorithm and present a case for geospatial resources for cognitive radio communications.**

***Index Terms*— Cognitive radio, interweave, dynamic spectrum access, network monitoring, 5G new radio, NR, opportunistic communications, energy detection, beamforming.**

I. Introduction

The adoption of cognitive radios increases spectrum efficiency [1]. However, many existing cognitive radio protocols are generic and do not address the constraints when applied to a specific wireless standard or radio access technology [2]. In theory, every wireless technology can leverage cognitive radio, and of the three cognitive radio paradigms, namely interweave, overlay, and underlay [3], at least one paradigm should fit with each technology, while the other paradigms may not be applicable at all. This paper focuses on cellular networks because of their broad impact on connectivity and applications [4]. Particularly, 5G NR is experiencing increased adoption. Hence, leveraging opportunities for 5G cognitive radio have been brought to attention [5].

The challenges when applying cognitive radio to a specific technology are further complicated depending on the secondary network's reliance on the primary network. Cooperation with the primary network prevents interference at the cost of increased network protocol complexity and additional dependence [6]. As defined in [7], a "self-reliant" cognitive network does not cooperate with the primary network with any feedback mechanisms or messages. Of the three paradigms, the interweave paradigm is the most reasonable for a self-reliant network because avoiding interference depends on dynamic spectrum access that only requires knowing network activity and not the contents of dynamically changing network messages [8]. Self-reliant cognitive networks provide communication opportunities without stipulations associated with the primary network, including infrastructure changes, standard adaptations, primary network control channel usage, and reliance on the primary network for all operations [7]. In addition, self-reliant communications can act as robust autonomous backup channels in case of primary network failure. Public safety is the primary application for these benefits, yet commercial applications also exist.

Recent studies show the importance of cognitive radio in public safety networks in the presence of cyberattacks [9], when a disaster strikes [10], and for supplementing the capabilities of existing networks [11]. If networks are vulnerable to outages, backup networks must not rely on those primary networks and conform to self-reliant standards. 5G public safety has focused on low-powered machine type communications (mMTC) using Category-M1 and Narrowband Internet of Things (NB-IoT) and their respective evolution in the 5G NR standard. However, mMTC has a very limited spectrum and requires control signals from the base station for resource coordination [12]. Additionally, 5G NR hopes to leverage Sidelink for both device-to-device (D2D) [13] and vehicle-to-everything (V2X) [14] communication so that devices can communicate without relaying commands through a base-station. However, the Sidelink resource pool limits the spectrum use and relies on the primary network for pre-configuration as well as initialization [15]. Resource pools are a pre-configured subset of resources that are subject to link failures, handover issues, and resource switching challenges [14]. In many proposed adaptations of Sidelink, the phrase "cognitive radio" has been used for overlapping topic areas such as network layer management and adaptable radio architectures [16]. Cognitive radio, in the context of this paper, reflects how secondary networks can coexist in a self-reliant manner with a primary network at the physical (PHY) and medium access control (MAC) layers.

Contribution: As of the writing of this article, no studies have considered self-reliant cognitive radio that fully considers the 5G NR standard. In [7], we developed CIAO-LTE, a methodology for establishing a self-reliant secondary network for 4G LTE. In this article, we adopt such a methodology for 5G NR. The MAC for multicast data can be used as stated in [7] while considering many of the same limitations, such as the short time transition interval and a low number of contention windows that persist in 5G. Only slight changes to the MAC are

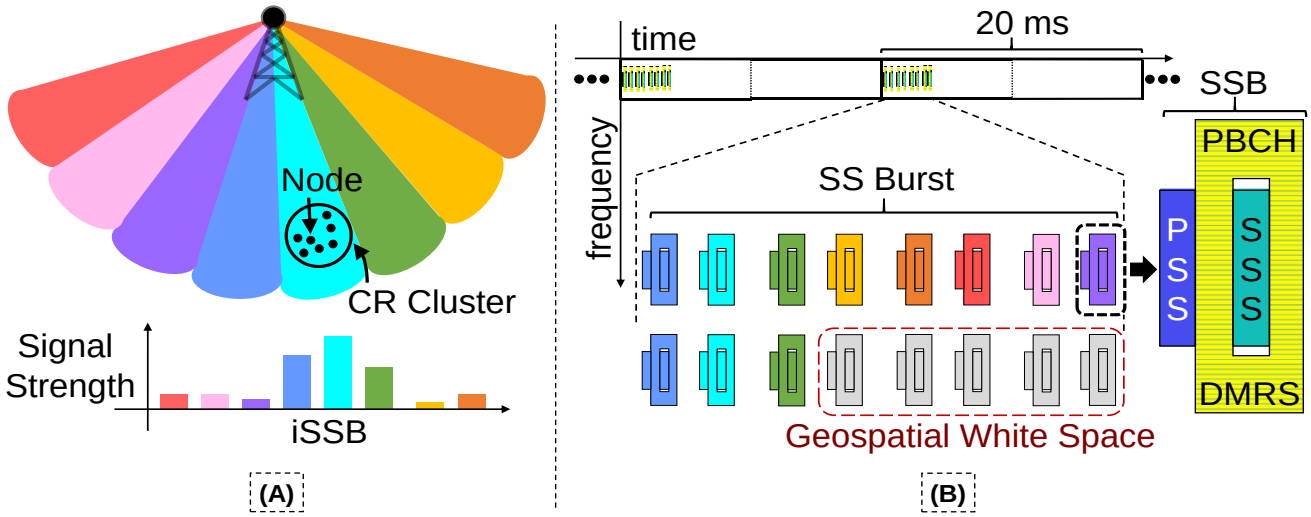

Fig. 1: 5G NR beamforming with CR cluster deployment (A) and SSB with geospatial white space (B).

required that are described in Section III.A. However, there are significant updates required for the PHY and resource detectors to leverage 5G beamforming waveforms. In this article, we opt to harness opportunities in 5G while avoiding the new physical layer security changes in the standard by introducing the Cognitive Algorithms for geo-Spatial Interweave Network Operations in 5G New Radio (CASINO-NR). CASINO-NR repurposes 5G NR synchronization signals as geospatial white space for the interweave paradigm while limiting interference on neighboring beams through novel beam detection and avoidance. CASINO-NR enables the creation of a multi-node cluster of collocated secondary nodes with mechanisms to control interference on a per cluster basis. The main contributions can be summarized as follows:

1) We develop a protocol for reusing 5G NR synchronization signals of non-neighbor beams that are geographically far away from secondary users. We avoid beams that are close to secondary users through beam sensing and ranking.
2) A power control protocol is designed to manage interference between the secondary and primary networks while considering 5G NR beamforming and subcarrier spacing variability. The geospatial reuse and power control protocols rely on beam avoidance to prevent the use and interference of neighbor beams.
3) We optimize beam detection and avoidance by using a combination of various reference signals, including a re-encoded information block concept.
4) Beam detection and ranking are further improved by comparing the various signal and noise plus interference (SINR) measurement techniques. We present a correlation-based technique that is more sensitive than other algorithms in literature.
5) We optimize beam detection under phase distortions expected in high frequencies of 5G NR. We propose channel equalization as a phase correction method in our beam detection and compare its performance against other mitigation techniques.

The simulation and experimentation results show the viability of CASINO-NR with beam detection sensitivity at -15 dB, outperforming alternative SINR and phase correction methods by 8 dB and 6 dB, respectively. Experimental results collected while traveling in a vehicle within a suburban area show 16.241 out of 32 beams found on average over 4.056 and 9.173 using alternative techniques. After power control and beam detection, potential throughput is estimated based on the experimental results. Of the 6.892 Mbps capacity with 64QAM and 32 beams, the experiment finds that CASINO-NR can support 1.507 Mbps per node during the test over 0.585 and 1.105 Mbps by other techniques. Lastly, our geospatial interweave concept has a more stable throughput than typical dynamic spectrum access, which often fluctuates in capacity based on the primary network's traffic. The next section discusses related 5G research.

II. Background and Related Work

Little research has explored self-reliant interweave networks for 5G NR. This section discusses published work on resource detectors, geospatial spectrum, and beam detection to satisfy this need.

Resource Detectors: Self-reliant networks require out-of-network detectors to determine resource availability without collaborating with the primary network. In both 4G and 5G, spectral resources are defined by physical resource blocks (PRBs) with symbols in time and subcarriers in frequency. The smallest spectral resource is a single symbol and subcarrier called a resource element (RE). Resource detection for spectral white space must be updated from 4G to 5G, as explained in our past work [17]. LTE and NR differ in a few ways. First, the NR PRB has a minimum duration of a single symbol providing higher flexibility than LTE. Second, instead of finding the control channels at the start of a time slot, the NR control channel can be placed in any PRB location within the channel [18]. Such flexibility makes isolating the NR control channel challenging for any user-specific control channels that do not have open access schedules [19][20]. Last, while LTE had fixed frequency carriers and defined resource grids, NR has bandwidth parts that dynamically adapt the bandwidth for a user within the frequency carrier.

Source	*Detector*	*Considerations*			*Comparisons*			
		Known Spectral Location & Signal Value	Constant Beam Orientation	High Layer Message Required	Chance to Cause Interfernce	Difficulty & Cost	Potential Throughput	Impacted by Traffic
[17] [22]	**Energy**	No	No	Yes** (SLIV/Mapping-Type)	High	Low	High***	Yes
[17] [23]	**Blind Control**	No	No	Yes** (RNTI/Scramble)	High	High	High***	Yes
contribution from this article	**Geospatial SSB**	Yes*	Yes	No	Low	Low	Low****	No
[24]	*Note: **	*Known after synchronization*						
[3GPP 138.321] [21] [3GPP 138.331] [24]	*Note: ***	*BWP info. from RRC messaging (sent per user on setup or encrpyted for reconfig), RNTI from RACH messaging (sent only on initial connect)*						
[20] [21]	*Note: ****	*FR1 (below 6 GHz): 11 to 273 PRBs, FR2 (above 6 GHz): 32 to 264 PRBs - Minus network traffic.*						
[20] [21]		*PRBs x 12 REs - Minus amount of reserved locations for CORESETs, SSBs, etc.*						
[24]	*Note: *****	*830 REs by #SSBs by Period*						

Fig. 2: Comparison of 5G NR detection schemes including energy detection, blind control channel detection, and the proposed geospatial SSB detection used in CASINO-NR.

NR flexibility hinders out-of-network resource detectors where control and data channel settings reside in higher layer messages within radio resource control information that is not accessible outside the network. Without these configurations, energy detectors cannot confirm if 5G resources start at fixed (Type A) or flexible (Type B) times or where white space can start or end in the latter case [21]. Recent work on energy detectors transitioning from 4G to 5G ignores this issue entirely [22]. 4G blind control channel detectors like [23], and designs that leverage them [17], also struggle to adapt to 5G without such higher layer information. As described in [17], the adaptation of blind control detectors to 5G NR is limited by unknown spectral location and configuration of user-specific control and data channels. Additionally, user-specific control messages in 5G are scrambled with the Radio Network Temporary Identifier (RNTI), which is unique for each user. The unknown scrambling ID and RNTI prevent the 4G blind detector from working on 5G [24][25]. In [26], the authors avoid these issues by getting configurations and scrambling IDs from in-network high-layer messages unavailable for out-of-network detectors and self-reliant communications. The aforementioned changes from 4G to 5G increase flexibility and security at the cost of the feasibility of adapting contemporary 4G blind control detectors, which motivates using known resources geospatially as an alternative to traditional white space.

Geospatial Spectrum: Geospatial use of spectrum has been demonstrated in [27], where beamforming increases the potential reuse of the spectrum geographically in cognitive radio environments [28]. However, no cognitive radio research has tried to use 5G NR synchronization signal blocks (SSBs) in this way. The SSB has a known value and spectral location after synchronization, which can be obtained with out-of-network information. Each SSB has a primary synchronization signal (PSS) and secondary synchronization signal (SSS), which collectively give a cell identity, a master information block (MIB), and the newly added demodulated reference signals (DMRS) [24], as seen in Fig. 1(A). Additionally, NR supports beamforming, where coherent signals are concentrated towards a specific azimuth to improve power ratios and throughput, especially important to overcome path loss at mmWave frequencies around 28 GHz and higher. As seen in Fig. 1(B), an SSB is sent uniquely for each beam where collectively, the group of SSBs is called the synchronization signal burst (SS Burst). The SSB cannot overlap with other NR waveforms as defined in [21]. At synchronization, the beam index (iSSB) is found by users and sent to the base station, which can then direct information to the user for improved performance. From there, additional tightening of the beam pattern can occur using a process called beam refinement [24]. Geospatial white space occurs when some beams are far enough away from a cognitive cluster, and their SSBs are at the noise floor, as seen in Fig. 1.

Fig. 2 shows tradeoffs between energy, blind control channel, and geospatial SSB reuse with green for advantages and red for disadvantages. Both energy and blind detectors require high-layer messages in 5G that are not available for out-of-network detection. However, this is not an issue with the geospatial SSB reuse concept because all SSB locations and their values are known after synchronization. Energy and blind detectors leverage the larger data channel in 5G; however, they do not predictively repeat and have unknown beam orientation, unlike SSBs that typically repeat every 20 ms and are guaranteed to only be given to a single beam. Geospatial SSB reuse also should at least operate down to the traditional cell search sensitivity at around –5 dB [29] over energy and blind detectors, which only operate down to around 7 dB and 10 dB [17], respectively, leading to better sensitivity and easier interference control. The geospatial SSB concept has overall easier interference management, lower complexity, and is not impacted by dynamically changing traffic at the cost of potential throughput, as seen in Fig. 2. However, a major concern with the geospatial reuse of beams is how to detect enough neighbor beams to make sure cognitive nodes only use beams that are far away and low risk of interference. This requires highly sensitive beam detection to rank beams for positional awareness [30] and confirm the absence of specific beams in a geographic area. Beam detection becomes more critical when considering that primary users can use multiple neighboring beams for increased diversity, and they too must be avoided [31].

Beam Detection: To enable highly sensitive beam detection and ranking, a parallel concept of upgrading a cell search to a detector [32] can be applied to beam search and detection where thresholds and optimizations are required to detect more than

one signal. Cellular waveform measurements include four different metrics for establishing connectivity, namely reference signals received power (RSRP), received signal strength indicator (RSSI), reference signal received quality (RSRQ) [33], and SINR recently added with the 5G standard [34]. This work focuses on SINR as it gives a clearer depiction of noise and interference than the other metrics. To estimate SINR, both the signal and the noise plus interference must be estimated. Noise and interference can be estimated with nulls or unused parts of the spectrum [35]. However, because of the flexibility of NR, there are a limited number of resource elements that can be guaranteed to be empty. Instead, a common yet practical approach is using the least-squares (LS) estimate from both channel estimation [36] and practical MMSE equalization [37]. The LS estimate is long-established and, through averaging, can be used to estimate the channel noise [38]. The signal component can also be found using the channel estimation, which is referred to as the *L-method* [39]. The RSRQ and the load of the network estimate an SINR, which we call the *Q-method* [40], where RSRQ contains both RSRP and RSSI [41]. In [42], RSRP is the signal component of SINR. However, RSRP does not have a clear definition in the 3GPP standard. Typically, RSRP is a power measurement of the received signal, which we call the *P-method* after combining with the LS estimate to find the SINR [43]. RSRP has also been related to correlation instead of a simple power measurement [44] and is applied as the signal component of the *C-method*.

All methods previously described and the LS estimate use some known reference signal. In [32], the approach only correlates with the PSS. Wang et al. [45] consider both PSS and SSS as reference signals in NR synchronization. In the 3GPP 5G NR standard, the DMRS is primarily used, and the SSS is secondarily used for beam measurement called the synchronization signal SINR (SS-SINR) [34]. However, CASINO-NR considers the combinations of multiple references as a longer length and higher gain reference signal and incorporates more than the DMRS and SSS. Such a combination is possible because CASINO-NR assumes synchronization to a primary beam has already occurred. So, the PSS, SSS, and DMRS are all known for any additional beams from the sector. Additionally, our approach will look at pre-coding the MIB of the primary beam to increase the correlation gain further for all synchronization beams, which has not previously been proposed. Doing so requires updating some fields such as frame number and re-encoding.

Beamforming typically occurs at higher frequencies, such as in mmWave in 5G NR. At these frequencies, phase noise and errors are common [46] and usually increase [47]. Phase error comes from residual carrier frequency offsets, oscillator phase misalignments, channel variations [48], multipath [49], and analog mixing [50]. The estimation of phase noise and error has been considered for cellular signals [51], where some studies assume coherency [52]. Another approach is to break up the correlation into subsets or parts that are coherent over a spectrum window where the channel frequency response is constant and then incoherently added together. The *subset* approach [53] uses a common window size of 12 subcarriers and 14 symbols, which was verified during testing [54]. Du and Zhu [55] use differential correlation to combine neighboring resource elements to correct phase distortions, called the *differential* approach. Both the subset and differential approaches have been applied to 4G LTE synchronization signals in [56]. Lastly, channel equalization has been used to improve correlation results and is proposed as the *equalization* approach [57]. The subset, differential, and equalization approaches are compared to determine the best phase correction in Section IV of this paper. These phase mitigation techniques are applied to the signal component of the *C-method* for SINR estimation and with all combinations of reference signals within the SSB. The following section looks at how the related work can be built upon to create CASINO-NR.

III. Detailed CASINO-NR Design

In this section, we detail the challenges and approach for CASINO-NR to support the geospatial use of synchronization signals in 5G, including beam selection and detection.

A. System Model and Design Goals

CASINO-NR targets the NR SS burst on the downlink for reduced complexity, a more stable resource pool, lower interference potential, and self-reliant cognitive radio development, avoiding the issues with energy and blind traffic monitoring in 5G. The main goal of CASINO-NR is to find SSBs available for reuse in a geographical area for secondary communications. Fig. 3 shows the system model for CASINO-NR with each required step illustrated as a functional block, deployment example, and timing increment from left to right. The required steps for the CASINO-NR algorithm include primary beam search, neighboring beam detection, geospatial beam selection, power control, and MAC protocols for cognitive radio resources. The main contributions of this work are optimizing beam detection and designing geospatial beam selection. Power control and MAC protocols are adapted from previous work.

CASINO-NR must consider preventing interference with other neighboring waveforms in the 5G NR channel. The properties of orthogonal time-division multiplexing (OFDM) limit the range of cognitive radio use of the spectrum. The edge of orthogonality (EoO) is defined as a radius around a secondary cognitive radio node, where there is no inter-symbol interference (ISI) and inter-carrier interference (ICI) when operating within white space [58]. The EoO is dependent on the cyclic prefix (CP), which acts as a guard time where the back portion of some symbol "x" is copied to the beginning of "x" The CP duration in 5G varies with subcarrier spacing and requires adaptation. This work adapts power control from our previous work, CIAO-LTE [7], to limit interference outside the EoO and consider beamforming.

In CASINO-NR, which beams are available are subject to change as nodes move around to different small coverage areas. Hence, the smallest resource size is a single SSB. The SSB only has four symbols which are too few time divisions to support contention with collision avoidance. CASINO-NR adopts slotted aloha as the best fit MAC because of the small number of contention slots, short time transition interval, and the rigid OFDM structure. Slotted aloha proves to be quite effective for CIAO-LTE [7] for the same reasons. To adapt the throughput

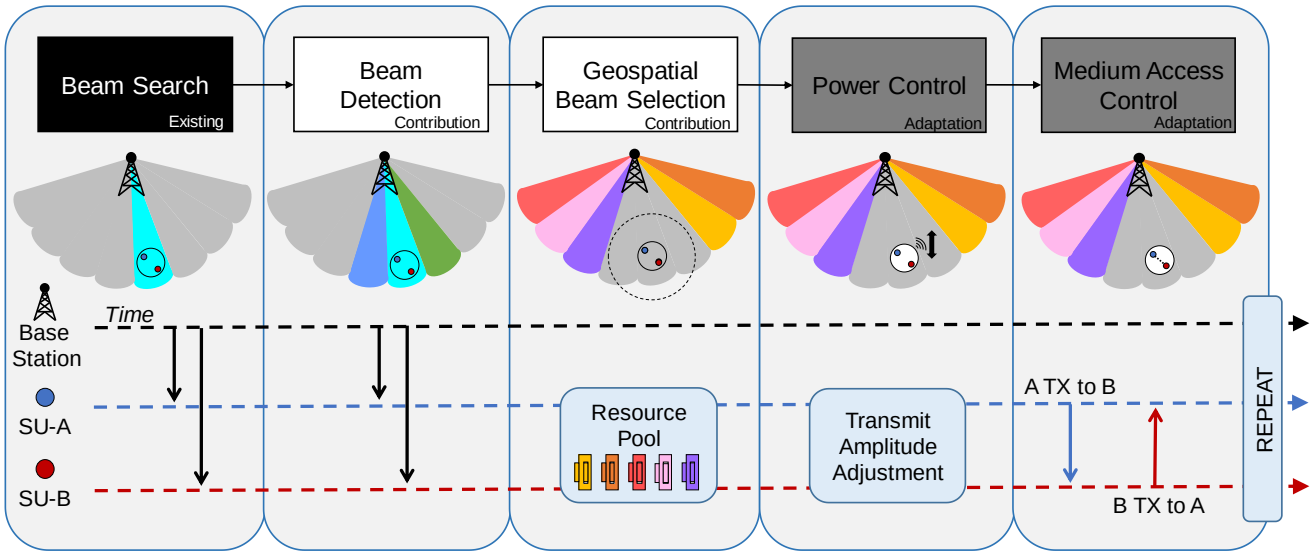

Fig. 3: System model for CASINO-NR showing high-level block diagram, cluster deployment example, and timing diagram. This example shows synchronization to the teal beam, detection of the blue and green beams, selection of all other SSBs, power control for secondary transmission, and communication with the adapted MAC protocol to create a supplementary link.

for slotted aloha, CASINO-NR does not need to consider the primary network load as seen by:

$$S_N = Ge^{-G} \times c_n \times \tau \times r\,, \tag{1}$$

where G is secondary traffic load, c_n is node connectivity, τ is transmitter detection rate, and r is receiver detection rate (the chance that the transmitter and receiver secondary nodes detect the same available beams). The throughput is based on the number of available beams (W_i), the number of resource elements of each beam (E), the modulation scheme (M), and the coding rate (C) that make up the number of bits per packet ($B = W_i \times E \times M \times C$) to convert to bits per second using,

$$S_N^+ = S_N B\,. \tag{2}$$

The system assumptions for CASINO-NR are as follows:

- CASINO-NR employs out-of-network detectors and self-reliant protocols. Out-of-network techniques include synchronization, decoding of broadcast system information, and geospatial awareness of beamforming waveforms.
- The initial beam search is not a contribution of this paper after already being established in literature. This work assumes channel information from the primary beam can be used in the beam detector with little concern of incorrect channel estimation after proper thresholding.
- CASINO-NR assumes some level of geospatial awareness that improves by optimizing beam detection and measurement to prevent interference. Pre-deployment mapping or post-deployment movement and evaluation provide this information but require optimal beam detection to be effective. The proposed design strives to compensate for insufficient geospatial awareness but not the total lack thereof.
- A cognitive radio device is assumed to be capable of estimating its proximity to the tower through either power measurements or GPS coordinates and uses such an estimate to determine rough beam coverage sizes.
- After beam detection and selection, CASINO-NR uses the MAC protocol designed in [7] for throughput estimation as a best-fit MAC protocol for NR's short TTI and the small number of time contention windows possible in an SSB.

Geospatial reuse of 5G NR SSBs requires novel geospatial interference protocols to prevent interference on neighboring beams, as seen in Fig. 3. In this scenario, the blue, teal, and green marked beams are within the range of interference of the secondary network. However, the yellow, orange, red, pink, and purple beams have available SSBs for a small geographic area where power control can prevent interference to the beams farther away from the cognitive cluster. Geospatial beam selection and interference control are necessary for secondary use of the SSBs. The main challenges for beam selection and power control are:

1) How to update the EoO for 5G NR's subcarrier spacing variability and find cluster sizes?
2) How to control the interference for a cluster under diverse geospatial beamforming?
3) How to determine beam selection and avoidance?

To avoid interference with primary users, CASINO-NR optimizes beam detection by comparing SINR estimation strategies, improving correlations with combined references, and comparing phase mitigation strategies. The main challenges for beam detection and optimization are:

4) What SINR algorithms to use for ranking and measuring beams?
5) Which reference signals to use for beam detection (PSS, SSS, DMRS, or MIB)?
6) How to improve beam detection under phase error and noise?

CASINO-NR addresses the aforementioned challenges through geospatial beam selection and beam detection optimization, as explained in the rest of this section.

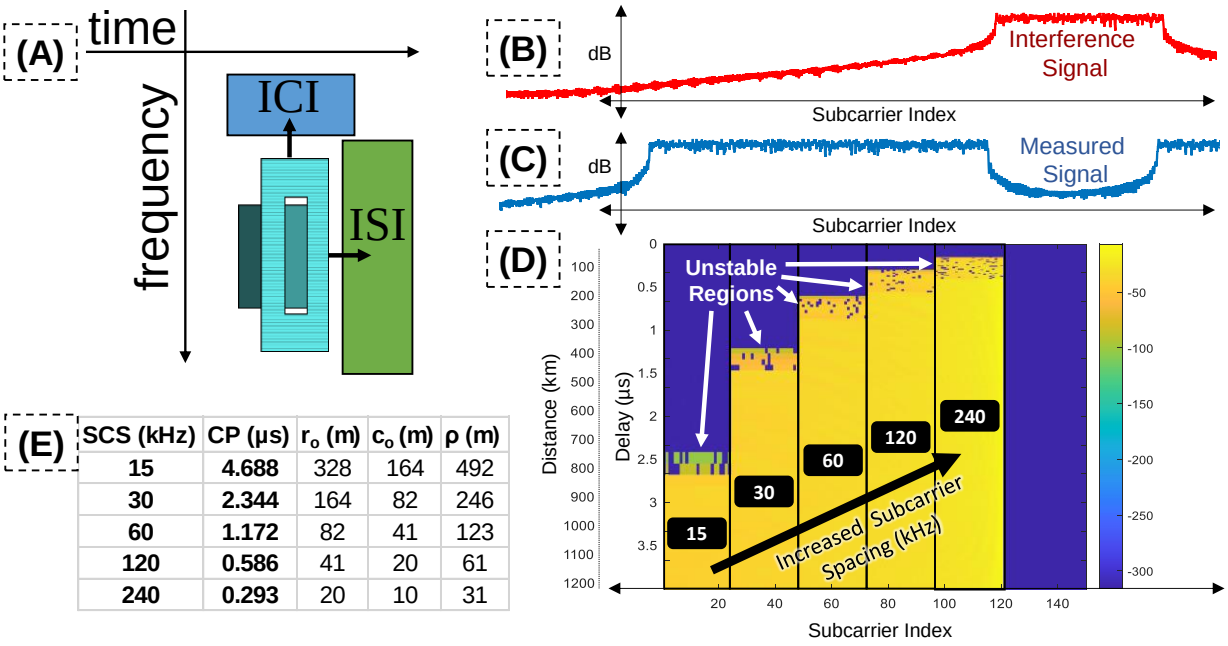

(E)

SCS (kHz)	CP (μs)	r_o (m)	c_o (m)	ρ (m)
15	**4.688**	328	164	492
30	**2.344**	164	82	246
60	**1.172**	82	41	123
120	**0.586**	41	20	61
240	**0.293**	20	10	31

Fig. 4: Interference considerations for orthogonal waveforms (A), interference signal (B), measured signal (C), showing ICI interference on measured signal with various delays on the interfering signal (D), and resulting maximum cluster sizes based on subcarrier spacing (E).

B. Geospatial Beam Selection

As previously stated, cognitive transmissions are only orthogonal at certain distances assuming a single beam. Additionally, Fig. 4(A) shows how ICI and ISI can occur on other beams where even though the SSB of the teal beam is being used, interference can occur on other neighboring beam waveforms if orthogonality is not preserved. The orthogonal range or EoO is defined by:

$$r_o = \frac{c\left(T_{CP} - \Delta\tau_{max}\right)}{2} \tag{3}$$

which is impacted by the speed of light (c), the cyclic prefix length (T_{CP}), and the maximum excess delay spread ($\Delta\tau_{max}$). The overall effective range comes down to comparing the cyclic prefix and spreading delay; the effective range is shown with varying interference and difference in path lengths in Fig. 4(D) with the interference signal seen in Fig. 4(B) and measured signal in Fig. 4(C). Though the interference and measured signal do not have overlapping subcarriers, they begin to interfere with one another at a maximum orthogonal path difference (OPD) [32]. The EoO is the OPD divided by two, which accounts for any user location by assuming the worst orientation and maximum delay between a cognitive radio transmitter and a synchronized base station [58].

In 5G NR, the EoO must consider the change in CP length found at configurable subcarrier spacing not found in 4G LTE. As the CP reduces, so do the excess delays expected in those scenarios. Based on [58][59][60], the expectation is that the maximum excess delay should scale with CP length to estimate the EoO (r_o), cluster radius (c_o), and the radius for severe interference of a cluster (ρ) in Fig. 4(E). The reduction of the CP in higher subcarrier spacing, found typically at high frequencies, diminishes the range of orthogonal transmissions, yet it increases the chances of geospatial reuse of the spectrum when leveraging empty beamforming assignments around the base station. The EoO considers a radius around a single node where ICI and ISI are zero between the node and the primary network. Communications can extend past the EoO but are subject to interference. The radius for an orthogonal cluster of nodes is then half the size of the EoO to guarantee every node in a cluster is orthogonal to each other as seen in Fig. 5(A). Other interference techniques that could increase the range such as cancellation carriers, guard intervals, and guard bands are not in the scope of this work.

Next, CASINO-NR addresses power control for overlapping sectors or beams while considering the EoO. First, the design must determine a distance to set power control for a cluster of nodes in Fig. 5(A) with the introduction of the edge of interference (EoI). The EoI or ρ is the radius from the cluster center where all nodes in the cluster begin to become non-orthogonal. At this radius, power control is not dependent on node distances, and a contention margin can be added to account for multiple interfering nodes, as discussed in [7]. Within the EoI, some interference occurs past the cluster, defined with radius (c_o), but interference increases as secondary transmissions combine closer to the EoI. Outside the EoI, all nodes interfere, and the EoI is the critical worst-case boundary to set power control that limits non-orthogonal interference. Fig. 5(B) shows how, based on the distance (d) and size of cluster interference, the angle at which a beam could perfectly cover a cluster can be calculated, where half this angle is ϕ. Determining this angle is critical in understanding how the EoI overlaps with potential neighbor beams.

To prevent interference, cognitive nodes must avoid beams that cross the EoI. Then power control will be performed at the EoI to limit secondary interference to primary nodes, similarly

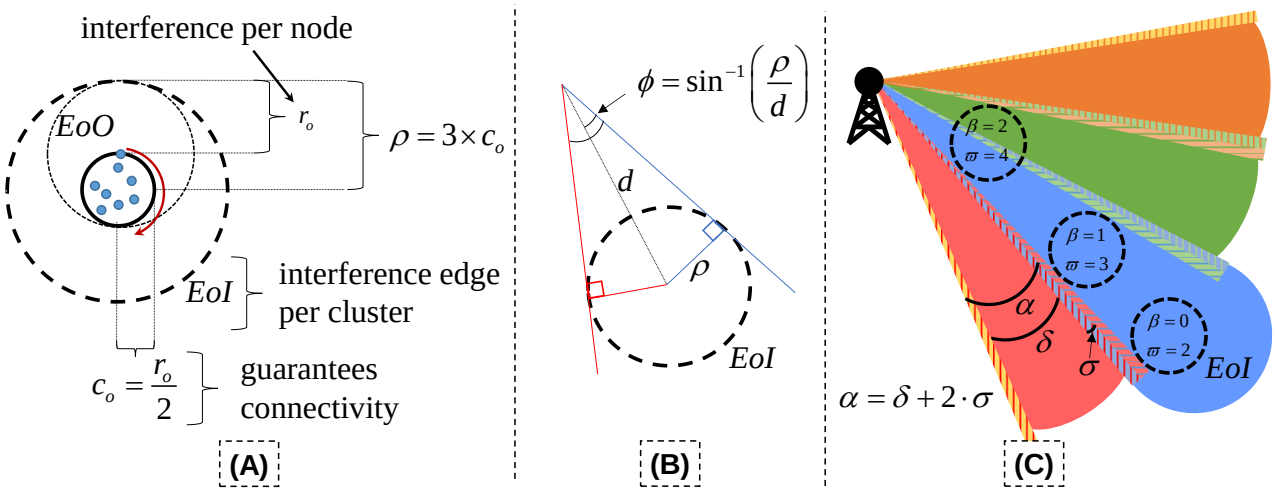

Fig. 5: Cluster interference dimensions for orthogonal waveforms (A), cluster interference angle of effect (B), and beam overlap interference mitigation (C).

to [7]. The number of neighbor beams within the secondary interference range comes from:

$$\beta = \sum_{z=1}^{Z} \left(z \cdot \delta + (n-1) 2 \cdot \sigma \right) < 2 \cdot \phi \tag{4}$$

where CASINO-NR assumes knowledge of the number of Z beams deployed using the system information block type 1 (SIB1) broadcast message field *ssb-PositionsInBurst*, with beam angles of α, beam overlap of σ, and beam angle without overlap of δ, as seen in Fig. 5(C). At a high level, (4) compares between two times ϕ versus α and δ or how many beams overlap the EoI. These parameters can be approximated with post-analysis of a beam deployment similar to the experimental results in Section V. Next, cognitive nodes must determine how many beams should be avoided to prevent interference to neighboring primary nodes (ϖ). The worst-case scenario is being on the beam edge and the edge of multiple layers of beams; it is thus assumed the farther from the tower a node is, the higher the chance that such a node will be in the next layer of beams. We then add an approximate number of reflected beams (k) that should be avoided, as seen by:

$$\varpi = \left[\underset{primary}{1} + \underset{neighbor}{1} + \underset{overlap}{\beta} \right] \times \left(1 + \underset{layer}{d / R_L} \right) + \underset{reflections}{k} \tag{5}$$

where R_L is the estimated size of the cell radius, and d is the distance to the cluster. Setting k reflected beams avoids beams from a non-direct line of sight. Next, the design counts the number of beams that pass threshold v depending on the SINR estimation described in the next section. Thus, the number of beams detected out of total beams (Z) is given by:

$$\upsilon = \sum_{z=1}^{Z} SINR(z) > v \,. \tag{6}$$

Cognitive nodes approximate the ratio of detected beams over the required number of beams using:

$$\Phi = \upsilon / \varpi \,. \tag{7}$$

Determining the number of available beams for secondary communications (W) is based on the total number of beams (N) minus the number of beams reserved (ϖ). Suppose the detection ratio is less than one. In that case, cognitive nodes can lower the chances of colliding with undetected beams by reducing the number of available beams through multiplication by the detection ratio:

$$W = \begin{matrix} if\,(\Phi >= 1) & N - \varpi \\ else & (N - \varpi) \times \Phi \end{matrix} . \tag{8}$$

This concept also decreases the number of beams available for secondary communications when too few beams are detected. It is assumed that the available beams are under some threshold to be considered white space for interweave cognitive radio. Such an assumption depends on the receiver sensitivity and other factors but works by setting a threshold on the available beams with a maximum SINR threshold (w), i.e.,

$$W_i = \sum_{n=1}^{W} SINR(n) < w \,. \tag{9}$$

Lowering α and δ in (4) can help in preventing interference by ultimately choosing fewer beams for secondary communication and handling insufficient beam information. Additionally, increasing the value of k in (5) increases the number of beams that must be avoided and lowers the ratio of detected beams over required beams in (7). Low values of Φ, especially under one, indicate too few beams have been detected and can trigger cognitive radios to halt transmission using (8).

In summary, CASINO-NR addresses the first set of challenges discussed in Section III.A by:

1) Defining the EoO and orthogonal cluster size based on the reduced CP guard time and expected delay spread with varying subcarrier spacing and expected multipath deployments.
2) Defining the EoI as a boundary to set interference control for a cluster of nodes and determining how many beams to avoid based on the overlap of the EoI with beam coverage.
3) Considering the number of possible beams detected to ensure a configurable number of beams are avoided.

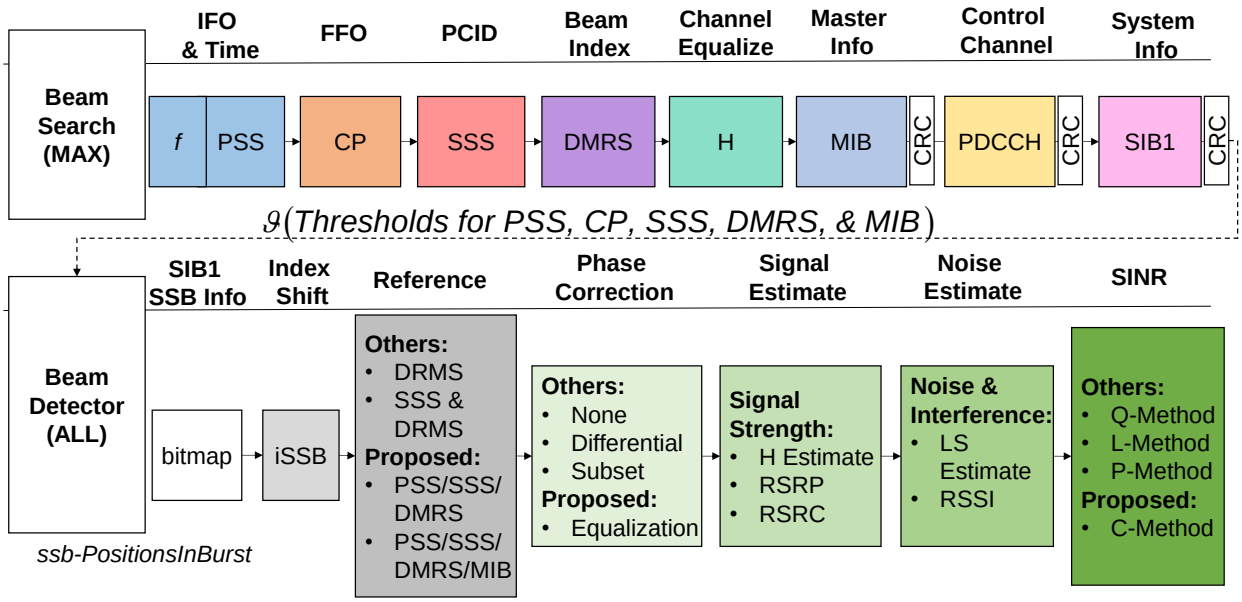

Fig. 6: Cell and beam search compared to beam detector with breakdown of different measurement algorithms.

Detection and ranking via SINR measurement are important to determine what beams are available for geospatial reuse and are the focus of the next subsection.

C. Beam Detection Optimization

After all parts of synchronization have met a collective group of thresholds (ϑ) for each synchronization step, the beam detector can be optimized using combinations of reference signals, SINR estimation methods, and phase correction techniques, as seen in Fig. 6. To understand the contribution, this subsection first presents a channel with x known transmitted signal, H the complex channel gain, n Gaussian noise, and y received signal seen in

$$y = H \cdot (x) + (n) = H \cdot (\xi \cdot \psi) + (\eta \cdot r). \tag{10}$$

Signal and noise power must be scaled to ensure accurate measurements for RSRP, RSSI, and RSRQ. The signal and noise power for x and n are scaled by $\xi = \sqrt{sinr_w \cdot noc}$ and $\eta = \sqrt{noc/2 \cdot N_{FFT}}$ from non-scaled versions ψ and r, respectively. Here $sinr_w$ is the linear SINR in watts, N_{FFT} is the fast Fourier transform size for the NR waveform, and noc is the linear noise power spectral density that is set based on the 5G NR standard [61]. The noc can also be approximated and scaled with live data if the noise variance is isolated without a signal or through the LS estimate, as discussed in the related work.

Next, the discussion shifts to how to optimize SINR and the related measurement statistics, where it is assumed that synchronization has been achieved to align to the SSB and that Y and X represent known sequences after demodulation in the frequency domain. The typical calculation of RSRP is done by finding the resource element power with only the received sequence using:

$$rsrp = \frac{1}{N}\sum_{i=0}^{N-1} Y \times Y^{*}, \tag{11}$$

where N is the number of resource elements in the sequence length. Measurement statistics like RSRP are capitalized to designate dB or dBm or lowercase like *rsrp* to designate linear scale. The recommendation is to leverage the known information X with a correlation which is referred to as the reference signal receive correlation power (RSRC). RSRC gives element power using the cross-correlation of known and received signals by:

$$rsrc = \left| \frac{1}{N}\sum_{i=0}^{N-1} Y \times X^{*} \right|^2. \tag{12}$$

RSRC should produce more sensitive estimations because of the advantage of using a matched filter. Average symbol power or RSSI can be found using:

$$rssi = \frac{1}{S}\sum_{j=0}^{S-1}\left(\sum_{i=0}^{\Theta-1}\left|Q^2\right|\right), \tag{13}$$

where Q is the sequence of resource elements, Θ is the number of resource elements, and S is the number of symbols to average across. The RSRQ metric can use either *rsrp* or *rsrc*. RSRP did not produce reliable simulation results because RSRP and RSSI become similar in value, picking up all signal, noise, and interference so that RSRQ converges to the number of resource blocks (N_{RB}) as *rssi* and *rsrp* cancel each other out. Instead, in this work, *rsrq* is defined with *rsrc*, which provided more accurate results using:

$$rsrq = \frac{rsrc \times N_{RB}}{rssi}. \tag{14}$$

Now that all measurement statistics have been described, this subsection can look at varying SINR methods designated with key letters such as "Q" for RSRQ, "L" for LS channel estimate, "P" for power, and "C" for correlation. In the Q-method [40], RSRQ is related to SINR but depends on network load as seen by:

(A)

Carrier Settings						
ARFCN	Fc (GHz)	Band	SCS (kHz)	SS Block	IBW	Beamforming
2071387	27.53328	n261	240	Case E	100 MHz	32 out of 64 beams

Path Loss Model Settings					
gNB Model	CR Model	Parameters:	α	β	γ
Suburban ABG	Suburban ABG		2.29	28.6	1.96

Channel Settings			
Model	Delay Profile	Velocity (km/h)	Root Mean Square Delay (ns)
Tapped Delay Line	TDL-D (LOS)	96	30

Interference Model Settings				
CR Power (W / dBm)	BS Power (W / dBm)	CR # PRBs	Base Station # PRBs	# PRBs Notch
1/30	1/30	20	60	20

(B)

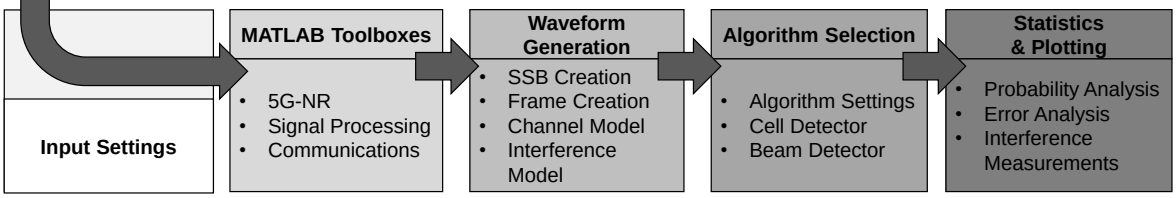

Fig. 7: Parameters for frequency carrier, path loss, channel, and interference model (A) and simulation test setup (B).

$$Q = sinr = \frac{U}{\frac{1}{12 \times rsrq_c} - U}, \tag{15}$$

where network load (U) for an SSB is one as every carrier is populated. The LS estimate of channel H can be found by:

$$\tilde{H} = \frac{Y}{X} = H + N, \tag{16}$$

where the channel estimation $\tilde{H}$ can be denoised by averaging using a smoothing window and interpolation $\tilde{H}_{AVG}$. The window size is to be optimized during simulation and testing. The noise and interference estimation can be found from their difference by [38]:

$$\tilde{N} = \tilde{H} - \tilde{H}_{AVG}. \tag{17}$$

The L-Method uses the LS estimate for the signal component [39] with:

$$L = sinr = \frac{\tilde{H}}{\tilde{N}}. \tag{18}$$

The P-Method uses noise estimate from the LS estimate and *rsrp* from above with:

$$P = sinr = \frac{rsrp}{\tilde{N}}. \tag{19}$$

The proposed C-Method uses noise from the LS estimate and the *rsrc*, specified above, using:

$$C = sinr = \frac{rsrc}{\tilde{N}}, \tag{20}$$

This provides four ways to measure SINR with the Q, L, P, and C methods.

Each method can use different combinations of reference signals for varying performance. As discussed in Section II, this work compares the traditional use of the PSS, SSS, and DMRS in beam measurement with combinations of sequences. Additionally, the MIB found in the primary beam is re-encoded and added to this known reference to find neighbor beams from the same sector for additional gain. Lastly, three methods of phase correction are used with the Q and C-method to account for phase noise and error, namely subset [53], differential [55], and equalization [57], which is recommended for the C-method. Each phase mitigation corrects the signal power under interference but negatively affects the sensitivity of the SINR estimate. Optimizing these SINR algorithms is key to avoiding neighboring beams and determining geospatial SSB reuse.

In summary, CASINO-NR addresses the second set of challenges in Section III.A by:

4) Introducing the C-method for SINR estimation and beam measurements.
5) Leveraging all possible references in the SSB, including the PSS, SSS, DMRS, and MIB, and combining multiple of these reference signals to provide higher gain and detection capabilities.
6) Improving beam detection by comparing the differential, subset, and recommended equalization phase mitigation techniques.

Next, we simulate beam detector methods and potential interference from CASINO-NR.

IV. Simulation Results

CASINO-NR is validated through simulation using Matlab 2020b, where a cell and a beam detector are implemented. The implementation also has modeled interference caused by CASINO-NR to evaluate the impact of beam selection and power control. Simulations ran over 1000 times with the parameters for path loss, channel, and interference modeling, produced results using parameters shown in Fig. 7(A), which mimic the suburban scenario found in the experimental results. Fig. 7(B) shows the simulation steps that include toolbox selection, waveform creation, channel effects, SINR setting, and the selection of algorithms and statistics for beam detection and interference modeling.

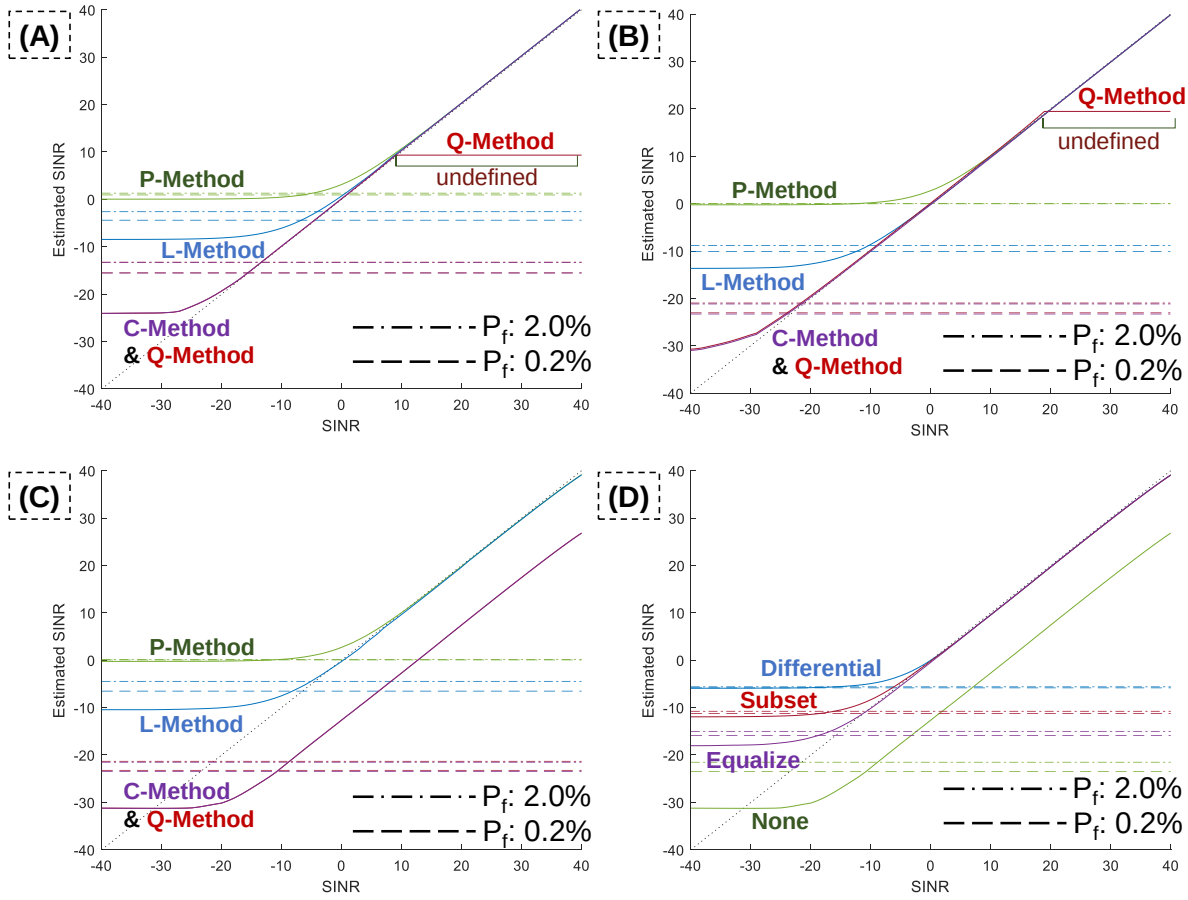

Fig. 8: Simulated sensitivity for SINR algorithms with no fading channel using DRMS (A), no fading channel using PSS, SSS, DMRS, and MIB (B), phase interference channel with PSS, SSS, DMRS, and MIB (C), and phase interference channel with C-Method using various phase correction techniques (D).

A. Beam Detector

Beam detection is critical for the performance of CASINO-NR and is validated through simulation. Fig. 8 shows various results of the SINR estimations under different noise levels. Methods P, L, Q, and C are shown in Fig. 8(A), with thresholds of the probability of false alarm of 2.0% and 0.2% found using the Monte Carlo method. Fig. 8(A) uses only the DMRS as the reference signal, whereas Fig. 8(B) shows the improvement when using the PSS, SSS, DMRS, and re-encoded MIB. Going from DMRS to all possible reference signals of the SSB shows a 1, 5, and 8 dB improvement in sensitivity for the P, L, and C-method, respectively. Indicating the importance of combining reference signals for increased sensitivity.

The Q and C-method both produce almost the same sensitivity curves because they both leverage *rsrc* and, under phase distortions in Fig. 8(C), deteriorate in performance using the same SSB reference signals as Fig. 8(B). The performance decrease for adding phase error is roughly 0 and 5 dB for the P and L methods, whereas the C method accrues 43% error in all SINR estimations. A fading channel with only phase errors is applied to keep the tested SINR constant while seeing the effect of phase interference using a tapped delay line (TDL). The P, L, Q, and C methods are defined in (19), (18), (15), and (20), respectively.

Additionally, at higher SINRs, the Q-method becomes undefined, as seen in Fig. 8(A) and Fig. 8(B), because the SINR is dominated by path loss [40]; hence only the C-method is plotted for phase mitigation in Fig. 8(D). In Fig. 8(D), the phase mitigation corrects the correlation results to properly estimate the SINR with sensitivities of -6, -12, and -16 dB for the subset, differential, and equalization methods, respectively. The equalization method elevates the C-method as the most attractive approach under noise and phase interference compared to the P, L, and Q methods.

Fig. 9 shows results for multiple combinations of reference signals, SINR methods, and phase mitigation techniques. The C-method is 12 dB and 11 dB more sensitive than the next best L-method with and without phase interference. The equalization approach reduces the percent error of the SINR estimate for the C-method with roughly 4 and 9 dB improvement over the subset and differential methods. Additionally, two equal power 20 dB SINR cell waveforms have been combined to show equal power cell-to-cell interference and the accuracy of the SINR estimate with each method considering an expectation of 0 dB SINR. The results show an expected close to 0 dB estimate of SINR with 3, 3, 0, and 0 dB estimates for the P, L, Q, and C methods, respectively.

Under No Phase Interference								
P_f = 0.2%	PSS	SSS	DMRS	MIB	SS/DMRS	PSS/SSS/DMRS	PSS/SSS/DMRS/MIB	Unit
Q-Method	-13	-13	-13	-19	-16	-18	-21	dB
L-Method	0	0	-3	-4	-7	-8	-9	
P-Method	0	0	1	1	0	0	0	
C-Method (None)	-13	-13	-13	-19	-17	-18	-21	
Differential	-4	-4	-3	-5	-5	-5	-5	
Subset	-8	-8	-3	-9	-6	-7	-10	
Equalize	-11	-11	-9	-15	-13	-14	-17	
	Discontinuous		% Error High SNR (PSS/SSS/DMRS)			% Error at P_f = 0.2% (PSS/SSS/DMRS)		Unit
Q-Method	Yes (max hold)		48			3		%
L-Method	No		1			18		
P-Method	No		1			100		
C-Method (None)	No		1			3		
Differential	No		2			36		
Subset	No		1			49		
Equalize	No		1			1		
Note:	*Q-Method puts a max hold on any discontinuous values*							
Under Phase Interference* **								
P_f = 0.2%	PSS	SSS	DMRS	MIB	SS/DMRS	PSS/SSS/DMRS	PSS/SSS/DMRS/MIB	Unit
Q-Method	-13	-13	-13	-19	-16	-18	-21	dB
L-Method	0	-1	1	6	-3	-4	-4	
P-Method	1	1	2	0	0	0	0	
C-Method (None)	-13	-13	-13	-19	-17	-18	-21	
Differential	-4	-4	-4	-5	-5	-5	-6	
Subset	-8	-8	-4	-9	-7	-8	-11	
Equalize	-11	-11	-8	-14	-11	-12	-15	
P_f = 0.2%	Fading Resistant		% Error High SNR (PSS/SSS/DMRS)			% Error at P_f = 0.2% (PSS/SSS/DMRS)		Unit
Q-Method	No*		137			76		%
L-Method	Yes**		2			31		
P-Method	Yes		1			103		
C-Method (None)	No		43			72		
Differential	Yes		2			57		
Subset	Yes		2			40		
Equalize	Yes		2			12		
*Note: **	*This is only true because the Q-Method is using RSRC, if RSRP or H was used than it would be yes*							
*Note: ***	*This is true because the L-Method corrects the channel with a built in window or subset to average over*							
*Note: ****	*Used a Tapped Delay Line Channel from the MATLAB NR Toolbox: tested both driving and walking doppler with similar results*							

Fig. 9: Simulated sensitivity and percent error for varying SINR algorithms, reference signals, phase correction techniques under both non-fading and fading channels.

For phase correction, techniques using the C-method -1, 0, and -1 dB were found for the subset, differential, and equalize approaches, respectively, showing that all methods can measure cell-to-cell interference at 1 to 3 dB of accuracy.

Receiver operating curves for our optimized beam detector is shown in Fig. 10. Fig. 10(A) shows the performance of varying SINR algorithms with all known reference signals and equalization. Fig. 10(B) illustrates the performance of the C-method with equalization and all known reference signals at varying SINRs and thresholds for the probability of detection (P_d) and false alarm (P_f). Performance with perfect detection occurs above -12 dB. The Q-method is not considered further in our results because of the discontinuous issues at high SINR and inferiority compared to the C-method, which leverages the same *rsrc* estimate. Now that beam detection is optimized, the next subsection examines the experienced interference when using CASINO-NR.

B. *Interference Modeling*

To limit and better understand the types of interference caused by CASINO-NR, this subsection models interference using the settings seen in Fig. 7(A). The simulations use a base station signal with 60 PRBs and a 20 PRB notch for SSB insertion. Additionally, Fig. 11 shows the interference results for CASINO-NR for a cognitive cluster and base station in a geographical area. A single cognitive user's interference is shown but can be replicated to estimate the effects of multiple collisions from multiple simultaneous transmissions.

R is defined for all subplots as the signal over interference ratio for a specific signal, either the base station or cognitive radio signal. The powers for the base station and cognitive radio signal are normalized to apply any scaling. For example, if the base station was twice the power, a factor of 3 dB could be applied when the base station's signal is measured in Fig. 11(A) and Fig. 11(C). Similarly, half the power or -3 dB could be applied when the cognitive radio's signal is measured in Fig. 11(B) and Fig. 11(D). Fig. 11(A) and Fig. 11(B) look at ICI on neighboring resource blocks outside of the SSB; such ICI is caused by the combining of non-orthogonal signals that occurs even when sensing is correct. The unstable region occurs when interference only occurs on some subcarriers, as seen in Fig. 4(D). Fig. 11(C) and Fig. 11(D) show the interference caused directly on the SSB. The beamforming template shown in these figures has the same angles as the experimental results. The template helps measure the interference when incorrectly using certain beams spread away from the cognitive cluster and highlights the importance of beam ranking and avoidance of

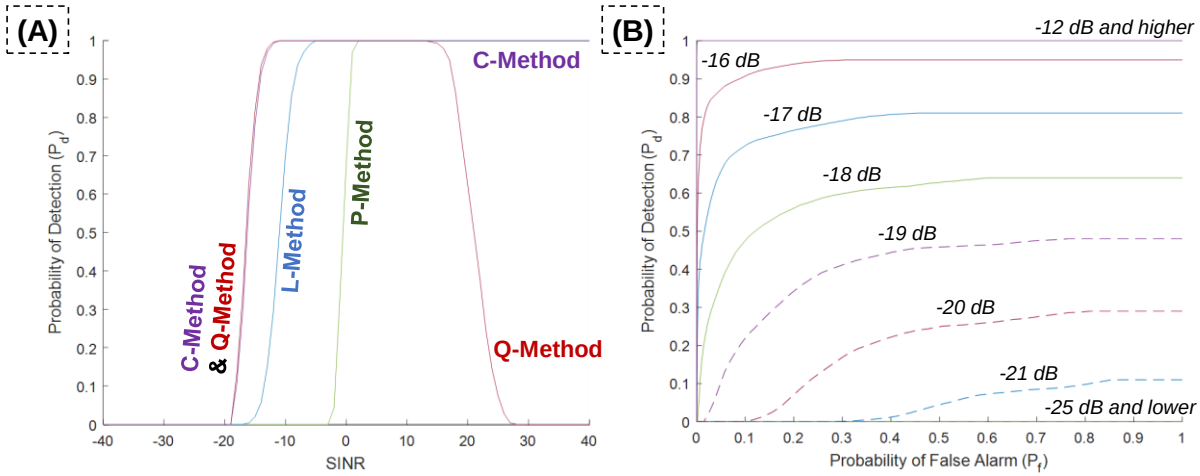

Fig. 10: Receiver operating curves under phase interference channel using PSS, SSS, DMRS, and MIB for SINR algorithms with equalization (Pf=0.2%) (A), and for only the C-method (Pf varies) (B), assuming at least 3 dB SINR measurement accuracy.

neighbor beams in proximity to the cluster. In the worst case, direct interference is 10 dB more than ICI because of the roll-off power on neighboring resources. Beam avoidance and power control can help control both interference types.

V. Experimental Results

This section validates the effectiveness of CASINO-NR using experimental live commercial network data recorded around the Baltimore/Washington International (BWI) Thurgood Marshall Airport in Baltimore, MD, USA. Waveforms were captured from a vehicle at varying geographical locations and subsequently processed with test equipment to determine beam layout and angles for geospatial beam avoidance and to test the beam detector.

A. Setup and Deployment

An Infovista TEst Mobile System (TEMS) was used to verify the Verizon 5G Absolute Radio Frequency Channel Numbers (ARFCNs) and instantaneous bandwidths (IBWs) of the downlink carrier with settings listed in Fig. 12(A). The ARFCN used by the TEMS phone was at 27533.28 MHz and was tested in the experimental results. Then, as seen in Fig. 12(B), mmWave waveforms were captured using a Rohde & Schwarz spectrum analyzer and sent to a laptop for processing using the Matlab software developed in the simulation setup, which provides subcarrier spacing, SS block type, and synchronization results.

Additionally, the power control analysis in Fig. 12(A) includes gNB and cognitive radio settings that are assumed reasonable for deployment in the considered suburban area and the experiment. Specifically, the gNB transmit power [62], the ABG model for suburban path loss [63], and the increased SINR requirement for 256-QAM [64]. Antenna height and cell radius were estimated based on the experimental results and Google Maps imagery. Some settings are configured based on [7], such as cluster connectivity (c), antenna gain, and maximum coding rate since they are not expected to change. These results used 64QAM for the secondary network and a

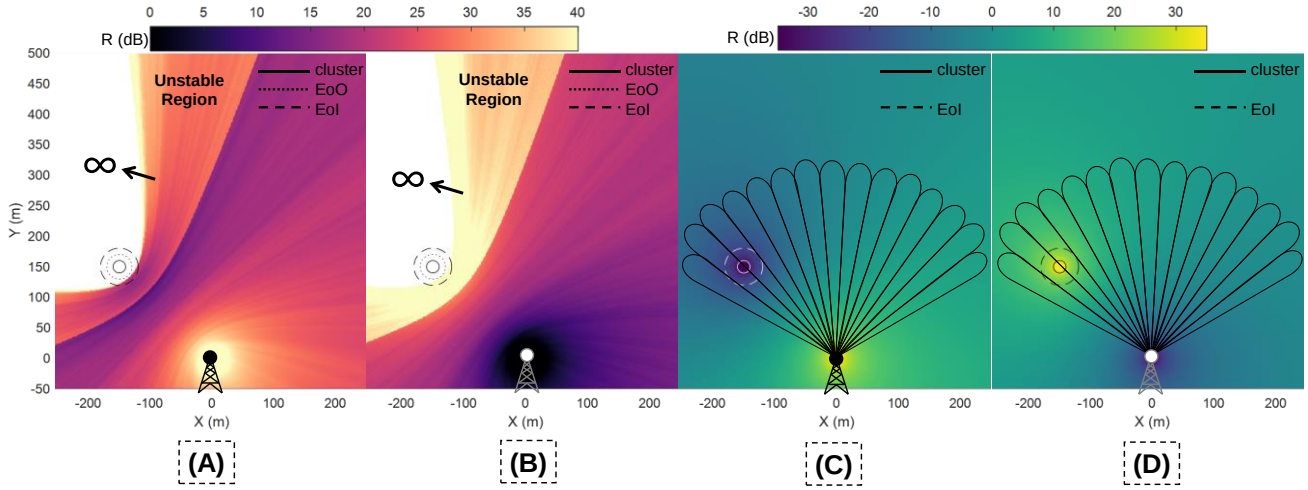

Fig. 11: Signal to interference ratio "R" over a geographical area on neighboring resource blocks for base station (A), cognitive radio signal (B), R from incorrect sensing on SSB resource blocks for base station (C), and cognitive radio signal (D) assuming normalize transmit power and a single CR transmitter centered in the cluster.

(A)

Carrier Settings						
ARFCN	Fc (GHz)	Band	SCS (kHz)	SS Block	IBW	Beamforming
2071387	27.53328	n261	240	Case E	100 MHz	32 out of 64 beams

Path Loss Model Settings					
gNB Model	CR Model	Parameters:	α	β	γ
Suburban ABG	Suburban ABG		2.29	28.6	1.96

Power Control Settings			
gNB Settings		CR Settings	
Antenna Gain (dBi)	15	Antenna Gain (dBi)	-1
Max. Power (W / dBm)	20/43	Max. Tx Power (mW)	1
Max. Modulation	256-QAM	Max. Modulation Possible	64-QAM
Required SINR for UE (dB)	33	Edge-to-Edge Cluster Power	-91 dBm
Tower Height (m)	45	Cluster Connectivity "c"	93%
Cell Radius (m)	250	Critical Coding Rate "C"	93%
Deployment Mode	Non-Stand Alone	Edge of Orthogonality (m)	20
Provider	Verizon	Contension Margin "M" (dB)	3

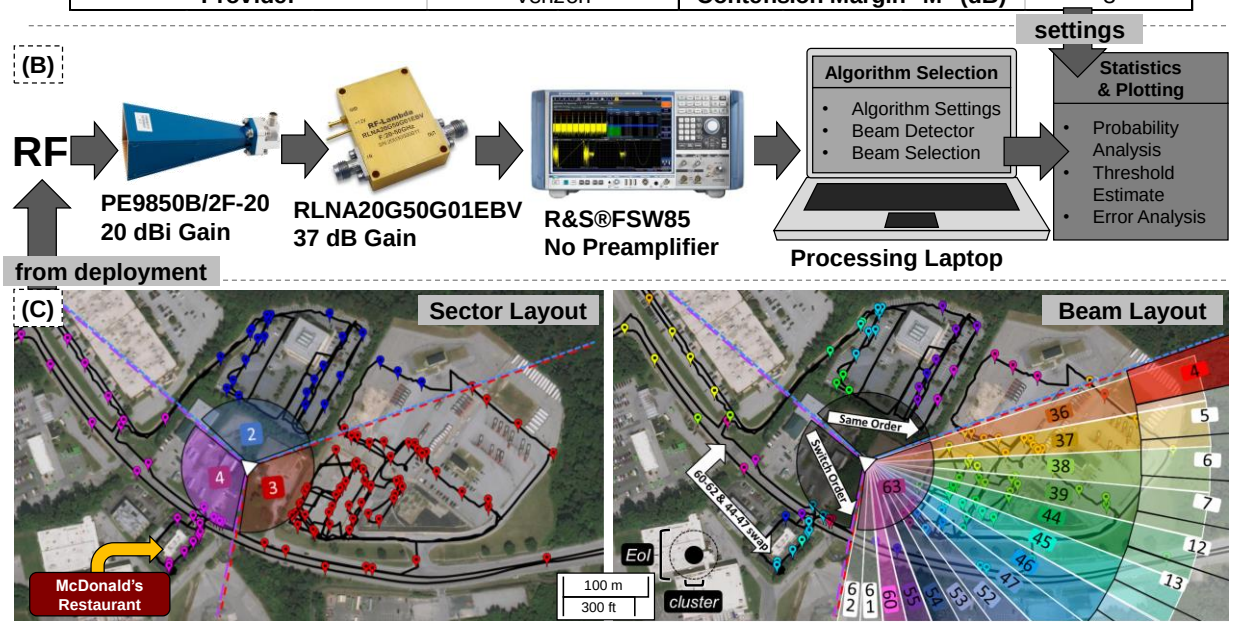

Fig. 12: Experiment parameters for frequency carrier, path loss, and power control settings (A), experimental test setup (B), and network deployment at the BWI Airport small cell (C). Imaging from Google Maps.

contention margin of 6 dB to handle collisions for up to four simultaneously transmitting nodes. The maximum transmit power for cognitive nodes was set to 1 mW adapting the power control equations to the 5G mmWave changes and BWI test site. In Fig. 12(C), experimental results from our detector show the data collection map for sector layout (A) and beam deployment (B) for the small cell near BWI. An approximation of the beam layout was confirmed with the TEMS device and matched the orientation found in other 5G mmWave deployments [65] with similar beam spacing and numbering. Additionally, (C) shows the EoI and cluster size for 240 kHz subcarrier spacing which covers the area of the McDonald's Restaurant shown in the picture.

B. Beam Detector

Geospatially reusing the SSB in neighboring beams requires optimized detection and ranking to find and eliminate beams subject to cognitive interference that could diminish primary user communications. Fig. 13(A) shows the beam pattern indices for SSBs, where 32 of 64 possible beams are active. The beam layout has pattern 1b00001111 and repeats eight times. Fig. 13(B) presents an example of one geographical location where beam #44 is the primary beam, and other beams range from the power of beam #44 to the noise floor. The colormap in (B) uses the SINR P-method for each resource element (P_{RE}) without averaging like in RSRP. At this location, cognitive nodes will synchronize to beam #44 and then use all known SSB references based on beam #44 to measure neighboring beams which will be avoided for cognitive communications. Any leftover beams that are active but ranked low, have SINR under a 1 dB threshold used in (9), and are deemed to be far enough from the cognitive nodes may be reused with little interference.

In Fig. 13(C), the C-method SINR estimation is shown with varying phase mitigations where equalization has the best sensitivity while also correcting the C-method estimate. With no phase correction, the C-method estimates diminish, losing accuracy compared to the expected SINR. All phase corrections

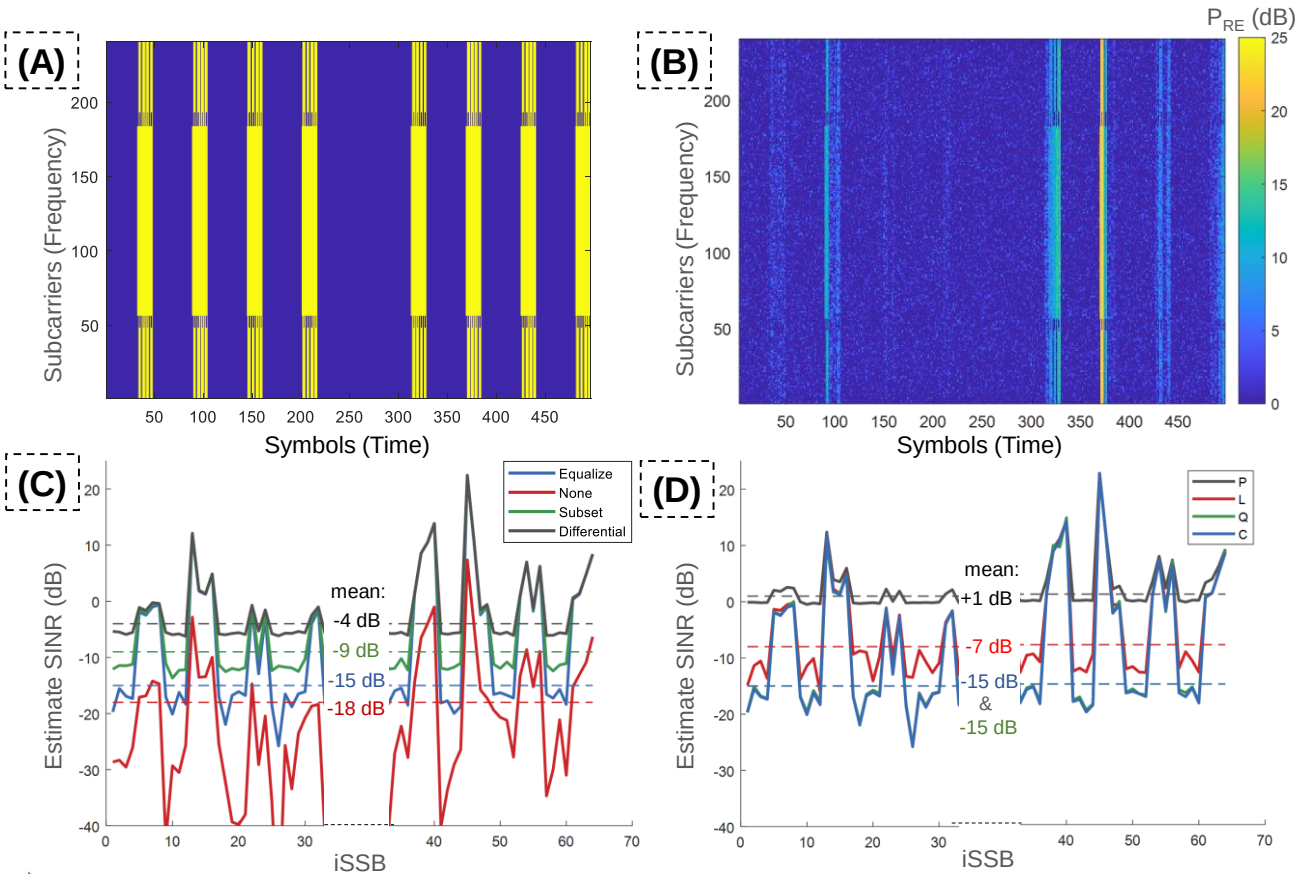

Fig. 13: Simulated SSB beam pattern with indices in yellow (A), matching experimental waveform (B), phase correction techniques for C-Method (C), and comparison of SINR algorithms using all possible reference signals (D).

increase the estimated threshold but fix the SINR estimation, similar to the simulation results. In Fig. 13(D), each method is compared with the optimized C-method. The Q-method is not considered for the rest of the experimental section as it had similar sensitivity as the C-method but with unknown estimations under high SINR. The C-method has similar improvements over the L and P-methods as previously seen in the simulation results in Fig. 9 and verified in the experimental data in Fig. 14. The equalize approach has 6 dB and 11dB better sensitivity than the subset and differential techniques, respectively. The C-method using equalization has an 8 dB improvement over the L-method and 16 dB over the P-method, matching the simulation results. Roughly a 3 dB decrease in sensitivity is found between the simulation and field experiment, which is expected as an implementation margin [19]. Lastly, Fig. 15 shows the results for the P-, L-, and C-methods over the route marked in black. Fig. 15(A) includes a comparison, where the P, L, and C-method find an average of 4, 9, and 16 of 32 beams, respectively. Fig. 15(B), (C), and (D) show the P, L, and C-method beam detection heat maps, respectively, where darker blue indicates higher and lighter yellow fewer beam detections.

C. Throughput Estimation

Fig. 16(A) shows the angles to the possible cognitive radio cluster at each point in the test area relative to the closest tower using variables shown in Fig. 5 (ϕ, α, and δ). These impact how many neighbor beams overlap with the EoI from (4), where Fig. 16(B) shows the number of beams that must be avoided from (5) based on the number of overlapping neighbor beams (β) and the number of available beams (N - ϖ) from (8). In Fig. 16(C), the Φ factor from (7) is shown for each method, where one means that enough beams are detected to avoid interference. The detection requirement is met 35.3%, 66.24%, and 90.2% of the time during the test for the P-, L-, and C-methods. Based on the power control settings in Fig. 12(A) and the Slotted Aloha MAC protocol adapted in our previous work [7], the max throughput from (1) and (2) is estimated in Fig. 16(D), where the number of beams is chosen based on (8) and (9). Having a more sensitive method ensures enough beams are found and avoided to prevent interference, and then more beams can be used safely for higher throughput, as seen in Fig. 16(D). Otherwise, the throughput diminishes as more beams are avoided to blindly lower the chance of collision. The C-method using equalization has outperformed the L and P-methods for SINR estimation.

VI. Conclusions and Future Work

This paper presents CASINO-NR, a practical approach for self-reliant cognitive radio in 5G NR. CASINO-NR avoids the challenges of 5G's increased complexity by leveraging geospatial SSBs as a new resource for secondary networks. We have demonstrated the effectiveness of the CASINO-NR approach with simulations and experiments. The simulation and

Experimental Static Data								
Threshold (P_f = 0.2%)	**PSS**	**SSS**	**DMRS**	**MIB**	**SS/DMRS**	**PSS/SSS/DMRS**	**PSS/SSS/DMRS/MIB**	**Unit**
L-Method	-1	-2	-2	-5	-6	-4	-7	**dB**
P-Method	1	1	2	1	1	1	1	
C-Method (None)	-10	-10	-11	-15	-13	-18	-18	
Differential	-4	-3	-3	-4	-4	-4	-4	
Subset	-8	-8	-3	-9	-6	-7	-9	
Equalize	-11	-11	-8	-13	-10	-11	-15	
% Error at High SNR	**PSS**	**SSS**	**DMRS**	**MIB**	**SS/DMRS**	**PSS/SSS/DMRS**	**PSS/SSS/DMRS/MIB**	**Unit**
L & P-Method	1	1	1	1	1	1	1	**%**
C-Method (None)	5	6	33	39	60	41	68	
Differential	1	1	1	1	1	1	1	
Subset	1	1	1	1	1	1	1	
Equalize	1	1	1	1	1	1	1	
SINR Above Threshold	**PSS**	**SSS**	**DMRS**	**MIB**	**SS/DMRS**	**PSS/SSS/DMRS**	**PSS/SSS/DMRS/MIB**	**Unit**
L-Method	24	25	25	28	29	27	30	**dB**
P-Method	22	22	21	22	22	22	22	
C-Method (None)	32	32	27	29	22	31	26	
Differential	27	26	26	27	27	27	27	
Subset	31	31	26	32	29	30	32	
Equalize	34	34	31	36	33	34	38	
Note:	*Q-Method is discontinous at high SNR and had similar issues as seen in simulation*							

Fig. 14: Experimental sensitivity and percent error for varying SINR algorithms, reference signals, phase correction techniques.

experimentation results validated that CASINO-NR optimized beam detection and reuse. We optimize the C-method for SINR detection under interference by using the equalize phase correction approach for an additional 6 and 11 dB over the subset and differential methods. Using the C-method gains an additional 8 and 16 dB over the L-method and P-method, respectively. The Q-method was found to have similar performance when using a correlation as the C-method but can have discontinuities. Lastly, using all known references, including the re-encoded MIB, gives an additional 4 to 5 dB improvement over using the SS and SS with DRMS. Our beam detector operates down to -17 and -15 dB in simulation and experiment, respectively.

Using optimized beam detection, we have adapted power control protocols to avoid critical primary beams. Average beam detection for each method across the experiment is 4.05, 9.17, and 16.24 of 32 beams for the P, L, and C-method, respectively. These results meet the detection requirement 35.3, 66.24, and 90.2 percent of the time during the experiment for the P, L, and C-method, respectively. The cluster throughput throughout the experiment is 0.585, 1.105, and 1.507 Mbps for the P, L, and C-method, respectively. The capacity for 32 SSBs is 6.892 Mbps which does not include the applied contention from the MAC protocol or avoiding detected beams.

Future work could use an overlay cancellation method instead of interweave to use beams that are higher power but

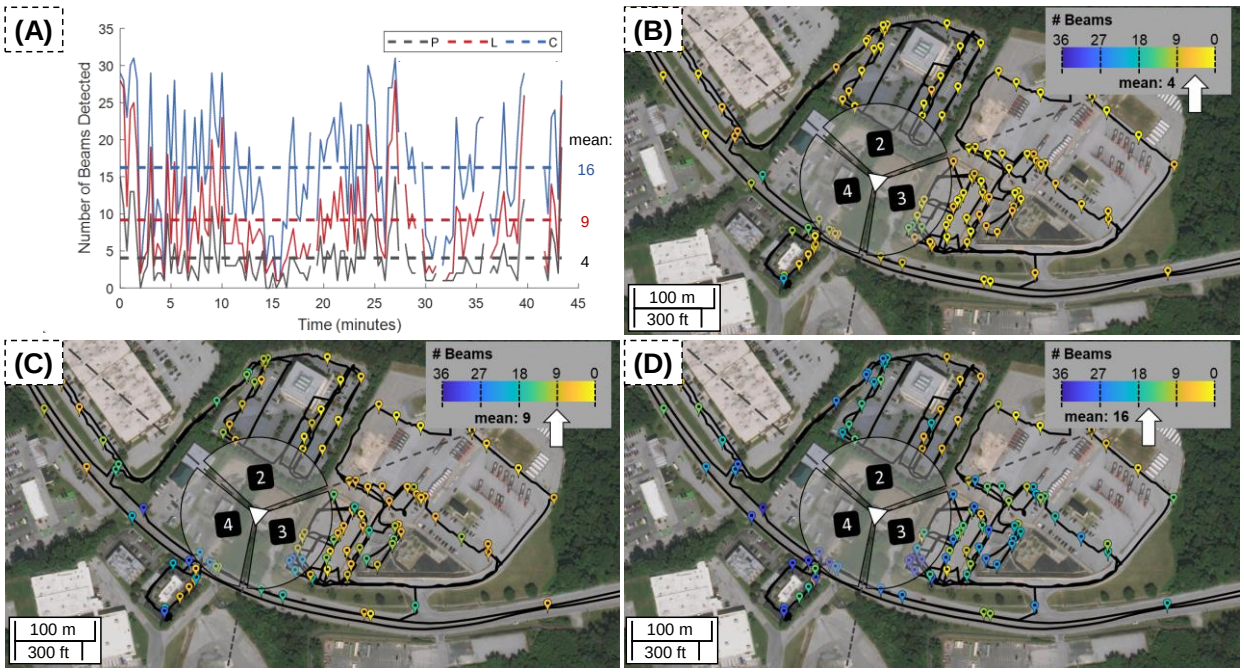

Fig. 15: Experimental test from a moving vehicle comparing detected number of beams (υ) with varying SINR algorithm (A), map of beam detections for P-Method (B), L-Method (C), and C-Method (D).

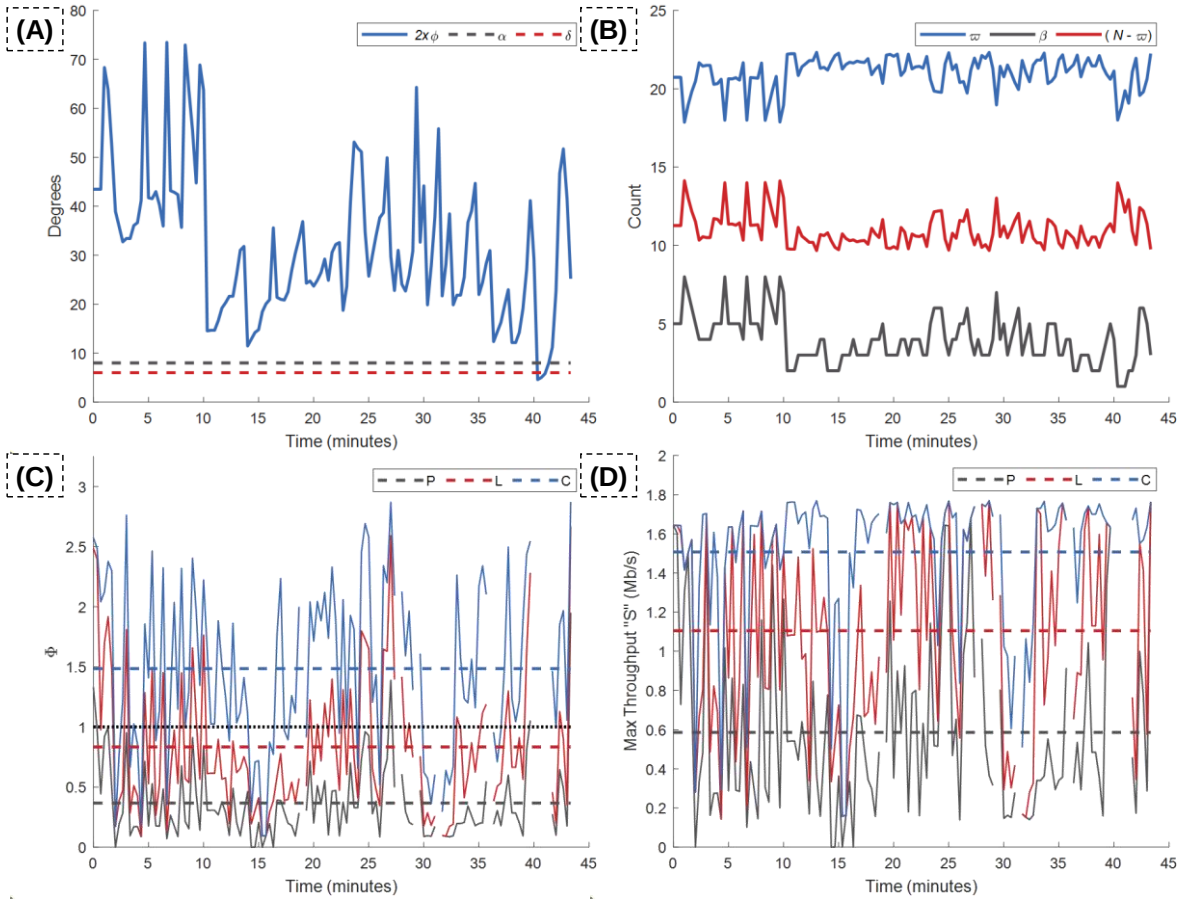

Fig. 16: Experimental test from a moving vehicle showing estimate and assumed cluster angles (A), spatially available beams with R_L as 250 meters and k as 2 (B), beam detection criteria (C), and maximum cluster throughput (D).

still far enough away from cognitive nodes. Cancellation carriers or guard bands could increase cognitive transmission range by trading off throughput. Self-reliant communication channels should be considered an essential addition to the overall cellular capabilities rather than a complete solution. For that, adaptations of network layer solutions to dynamically include self-reliant cognitive backup links is needed.

VII. References

[1] M. Singh, P. Kumar, and S. K. Paruthi, "Techniques for Spectrum Sensing in Cognitive Radio Networks : Issues and Challenges," *IRJET*, vol. 3, no. 5, 2016.

[2] T. V. Saroja and L. L. Ragha, "A Dynamic Spectrum Access Model For Cognitive Radio Wireless Sensor Network," in *International Conference on Electronics and Communication Systems*, 2017, vol. 1, pp. 105–112.

[3] A. Goldsmith, S. A. Jafar, I. Maric, and S. Srinivasa, "Breaking Spectrum Gridlock With Cognitive Radios : An Information Theoretic Perspective," *Proc. IEEE*, vol. 97, no. 5, pp. 894–914, 2009.

[4] G. A. Akpakwu, B. J. Silva, G. P. Hancke, and A. M. Abu-Mahfouz, "A Survey on 5G Networks for the Internet of Things: Communication Technologies and Challenges," *IEEE Access*, vol. 6, pp. 3619–3647, 2017.

[5] W. S. H. M. W. Ahmad *et al.*, "5G Technology: Towards Dynamic Spectrum Sharing Using Cognitive Radio Networks," *IEEE Access*, vol. 8, pp. 14460–14488, 2020.

[6] A. F. Tayel, S. I. Rabia, A. H. Abd El-Malek, and A. M. Abdelrazek, "Spectrum Access Management of Multi-class Secondary Users in Hybrid Cognitive Radio Networks," *IEEE Veh. Technol. Conf.*, vol. 2021-April, 2021.

[7] B. W. Stevens and M. F. Younis, "Physical Layer and MAC Design for Self-Reliant Cognitive Multicast Networks using LTE Resources," *IEEE Trans. Cogn. Commun. Netw.*, vol. 7731, 2020.

[8] W. Xu, R. Qiu, and X. Jiang, "Resource Allocation in Heterogeneous Cognitive Radio Network With Non-Orthogonal Multiple Access," *IEEE Access*, vol. 7, pp. 57488–57499, 2019.

[9] A. El-Keyi, O. Ureten, H. Yanikomeroglu, and T. Yensen, "LTE for Public Safety Networks: Synchronization in the Presence of Jamming," *IEEE Access*, vol. 5, pp. 20800–20813, 2017.

[10] A. Amrallah, E. M. Mohamed, G. K. Tran, and K. Sakaguchi, "Enhanced dynamic spectrum access in UAV wireless networks for post-disaster area surveillance system: A multi-player multi-armed bandit approach," *Sensors*, vol. 21, no. 23, 2021.

[11] A. Rahmati, X. He, I. Guvenc, and H. Dai, "Dynamic Mobility-Aware Interference Avoidance for Aerial Base Stations in Cognitive Radio Networks," *Proc. - IEEE INFOCOM*, vol. 2019-April, pp. 595–603, 2019.

[12] N. Varsier, L. A. Dufrene, M. Dumay, Q. Lampin, and J. Schwoerer, "A 5G New Radio for Balanced and Mixed IoT Use Cases: Challenges and Key Enablers in FR1 Band," *IEEE Commun. Mag.*, vol. 59, no. 4, pp. 82–87, 2021.

[13] M. Irfan, J. Sher, N. Ullah, M. Sulaiman, and J. Saleem, "5G Wireless Technology-An overview of the Current Trends," *Int. J. Comput. Appl. Technol. Res.*, vol. 5, no. 7, pp. 489–494, 2016.

[14] M. H. C. Garcia *et al.*, "A Tutorial on 5G NR V2X Communications," *IEEE Comm. Surv. Tutors*, vol. 23, no. 3, pp. 1972–2026, 2021.

[15] S. Y. Lien *et al.*, "3GPP NR Sidelink Transmissions Toward 5G V2X," *IEEE Access*, vol. 8, pp. 35368–35382, 2020.

[16] I. Rasheed and F. Hu, "Intelligent super-fast Vehicle-to-Everything 5G communications with predictive switching between mmWave and THz links," *Veh. Commun.*, vol. 27, p. 100303, 2021.

[17] B. W. Stevens, J. M. Ray, J. S. Everett, E. M. Daugherty, Y. Yang, and M. F. Younis, "Cognitive Resource Analyzer for Cellular Network Ecosystems," *IEEE Trans. Cogn. Commun. Netw.*, vol. 7731, no. c, pp. 1–1, 2022.

[18] K. Takeda, H. Xu, T. Kim, K. Schober, and X. Lin, "Understanding the Heart of the 5G Air Interface : An Overview of," *IEEE Commun. Stand. Mag.*, vol. 4, no. 3, pp. 1–8, 2020.
[19] M. Sesia, S., Toufik, I., & Baker, *LTE-the UMTS long term evolution: From theory to practice*, 2nd ed. U.K: Wiley, 2011.
[20] 3GPP, "138 213 - V15.8.0 - 5G; NR; Physical layer procedures for control," 2020.
[21] 3GPP, "138 214 - V15.2.0 - 5G; NR; Physical layer procedures for data," 2018.
[22] M. Wasilewska, H. Bogucka, and A. Kliks, "Federated learning for 5G radio spectrum sensing," *Sensors*, vol. 22, no. 1, 2022.
[23] B. Sliwa, R. Falkenberg, and C. Wietfeld, "Towards Cooperative Data Rate Prediction for Future Mobile and Vehicular 6G Networks," in *2020 2nd 6G Wireless Summit (6G SUMMIT)*, 2020, pp. 1–5.
[24] 3GPP, "138 211 - V15.2.0 - 5G; NR; Physical channels and modulation," 2018.
[25] C. Condo, S. A. Hashemi, A. Ardakani, F. Ercan, and W. J. Gross, "Design and Implementation of a Polar Codes Blind Detection Scheme," *IEEE Trans. Circuits Syst. II Express Briefs*, vol. 66, no. 6, pp. 943–947, 2019.
[26] I. Kim, J. Um, and S. Park, "SDR-based 5G NR Control Channel Analysis Equipment for Network Monitoring," *Int. Conf. ICT Converg.*, vol. 2020-Octob, pp. 1060–1063, 2020.
[27] G. P. Joshi and S. W. Kim, "A survey on node clustering in cognitive radio wireless sensor networks," *Sensors (Switzerland)*, vol. 16, no. 9, pp. 1–19, 2016.
[28] A. Nasser, H. A. H. Hassan, J. A. Chaaya, A. Mansour, and K. C. Yao, "Spectrum sensing for cognitive radio: Recent advances and future challenge," *Sensors*, vol. 21, no. 7, pp. 1–29, 2021.
[29] Y. Kryukov, D. Pokamestov, and E. Rogozhnikov, "Cell search and synchronization in 5G NR," *ITM Web Conf.*, vol. 30, p. 04007, 2019.
[30] E. Rastorgueva-Foi, M. Costa, M. Koivisto, K. Leppänen, and M. Valkama, "User Positioning in mmW 5G Networks Using Beam-RSRP Measurements and Kalman Filtering," *2018 21st Int. Conf. Inf. Fusion, FUSION 2018*, pp. 1150–1156, 2018.
[31] I. K. Jain, R. Subbaraman, and D. Bharadia, "Two beams are better than one: Towards reliable and high throughput mmWave links," *SIGCOMM 2021 - Proc. ACM SIGCOMM 2021 Conf.*, vol. 1, pp. 488–502, 2021.
[32] B. W. Stevens and M. F. Younis, "Detection Algorithm for Cellular Synchronization Signals in Airborne Applications," *IEEE Access*, vol. 9, pp. 1–12, 2021.
[33] W. Xu and X. Ma, "Correlation-based cell search and measurement for LTE and LTE-A," *GLOBECOM*, p. 3719, 2012.
[34] 3GPP, "138 215 - V16.2.0 - 5G; NR; Physical layer measurements," 2020.
[35] J. Fei, R. Guangliang, and Z. Zhe, "A new noise variance and post detection SNR estimation method for MIMO OFDM systems," *Int. Conf. Commun. Technol. Proceedings, ICCT*, no. 60602063, pp. 179–182, 2008.
[36] J. J. van de Beek, O. Edfors, M. Sandell, S. K. Wilson, and P. O. Borjesson, "On channel estimation in OFDM systems," *IEEE Veh. Technol. Conf.*, vol. 2, no. 1, pp. 815–819, 1995.
[37] M. Jie, Y. Hua, and L. Shouyin, "The MMSE channel estimation based on DFT for OFDM system," *Proc. - 5th Int. Conf. Wirel. Commun. Netw. Mob. Comput. (WiCOM 2009)*, pp. 18–21, 2009.
[38] M. R. Raghavendra, S. Bhashyam, and K. Giridhar, "Improving channel estimation in OFDM systems for sparse multipath channels," *IEEE Work. Signal Process. Adv. Wirel. Commun.*, vol. 12, no. 1, pp. 106–109, 2004.
[39] G. Kutz, N. Zach, A. Bar-Or, and K. Bezalel, "LTE measurements with CRS interference cancellation," *IEEE Commun. Lett.*, vol. 20, no. 10, pp. 2063–2066, 2016.
[40] C. Ide *et al.*, "Empirical analysis of the impact of LTE downlink channel indicators on the uplink connectivity," *IEEE Veh. Technol. Conf.*, 2016.
[41] F. Afroz, R. Subramanian, R. Heidary, K. Sandrasegaran, and S. Ahmed, "SINR, RSRP, RSSI and RSRQ Measurements in Long Term Evolution Networks," *Int. J. Wirel. Mob. Networks*, vol. 7, no. 4, pp. 113–123, 2015.
[42] A. R. Ramos, B. C. Silva, M. S. Lourenco, E. B. Teixeira, and F. J. Velez, "Mapping between Average SINR and Supported Throughput in 5G New Radio Small Cell Networks," *Int. Symp. Wirel. Pers. Multimed. Commun. WPMC*, 2019.
[43] S. Xue, W. Weidong, and Z. Yinghai, "SNR Estimation based on Sounding Reference Signal in LTE Uplink," *IEEE Int. Conf. Signal Process. Commun. Comput.*, no. 61001088, pp. 1–6, 2013.
[44] R. Pec, J. H. Choi, C. H. Park, and Y. S. Cho, "Synchronization method for long-term evolution-based machine-type communication in low-power cellular Internet of Things," *Int. J. Distrib. Sens. Networks*, vol. 12, no. 8, 2016.
[45] W. Wang, Y. Tong, L. Li, A. A. Lu, L. You, and X. Gao, "Near optimal timing and frequency offset estimation for 5G integrated LEO satellite communication system," *IEEE Access*, vol. 7, pp. 113298–113310, 2019.
[46] J. Oh and T. K. Kim, "Phase noise effect on millimeter-wave pre-5G systems," *IEEE Access*, vol. 8, p. 187902, 2020.
[47] C. De Lima *et al.*, "Convergent communication, sensing and localization in 6g systems: An overview of technologies, opportunities and challenges," *IEEE Access*, vol. 9, pp. 26902–26925, 2021.
[48] Y. Du, D. Rajan, and J. Camp, "Implementation and evaluation of channel estimation and phase tracking for vehicular networks," *2013 9th Int. Wirel. Commun. Mob. Comput. Conf. IWCMC 2013*, pp. 1263–1268, 2013.
[49] H. Dun, C. C. J. M. Tiberius, and G. J. M. Janssen, "Positioning in a Multipath Channel Using OFDM Signals with Carrier Phase Tracking," *IEEE Access*, vol. 8, pp. 13011–13028, 2020.
[50] S. Wu and Y. Bar-Ness, "Performance analysis on the effect of phase noise in OFDM systems," *IEEE Int. Symp. Spread Spectr. Tech. Appl.*, vol. 1, no. C, pp. 133–138, 2002.
[51] R. Stuhlberger *et al.*, "LTE-downlink performance in the presence of RF-impairments," *Eur. Microw. Week 2007 Conf. Proceedings, EuMW 2007 - 10th Eur. Conf. Wirel. Technol. ECWT 2007*, no. October, pp. 189–192, 2007.
[52] A. Omri, M. Shaqfeh, A. Ali, and H. Alnuweiri, "Synchronization procedure in 5G NR systems," *IEEE Access*, vol. 7, pp. 41286–41295, 2019.
[53] Y. H. You, J. H. Paik, C. H. Park, M. C. Ju, K. W. Kwon, and J. W. Cho, "Low-complexity coarse frequency-offset synchronization for OFDM applications," *IEEE Int. Conf. Commun.*, vol. 8, pp. 2494–2498, 2001.
[54] C. S. Park and S. Park, "Analysis of RSRP Measurement Accuracy," *IEEE Commun. Lett.*, vol. 20, no. 3, pp. 430–433, 2016.
[55] Z. Du and J. Zhu, "Improved coarse frequency synchronization algorithm with extended differential detection," *IEEE Wirel. Commun. Netw. Conf. WCNC*, vol. 1, pp. 470–474, 2003.
[56] J. I. Kim, J. S. Han, H. J. Roh, and H. J. Choi, "SSS detection method for initial cell search in 3GPP LTE FDD/TDD dual mode receiver," *2009 9th Int. Symp. Commun. Inf. Technol. Isc. 2009*, pp. 199–203, 2009.
[57] Z. Feng *et al.*, "Performance-Enhanced Direct Detection Optical OFDM Transmission With CAZAC Equalization," *IEEE Photonics Technol. Lett.*, vol. 27, no. 14, pp. 1507–1510, 2015.
[58] P. Karunakaran and W. H. Gerstacker, "Sensing Algorithms and Protocol for Simultaneous Sensing and Reception-Based Cognitive D2D Communications in LTE-A Systems," *IEEE Trans. Cogn. Commun. Netw.*, vol. 4, no. 1, pp. 93–107, 2017.
[59] V. Raghavan *et al.*, "Millimeter Wave Channel Measurements and Implications for PHY Layer Design," *IEEE Trans. Antennas Propag.*, vol. 65, no. 12, pp. 6521–6533, 2017.
[60] K. Hassan and T. A. Rahman, "The Mathematical Relationship Between Maximum Access Delay and the R . M . S Delay Spread," *7th Int. Conf. Wirel. Mob. Commun.*, pp. 18–23, 2011.
[61] 3GPP, "138 533 - V15.1.0 - 5G; NR; User Equipment conformance specification; Radio Resource Management," 2019.
[62] 5G Americas, "Understanding mmWave Spectrum for 5G Networks," 2020.
[63] Y. Zhang *et al.*, "28-GHz Channel Measurements and Modeling for Suburban Environments," *IEEE Int. Conf. Comms.*, 2018.
[64] D. F. Carrera, C. Vargas-Rosales, N. M. Yungaicela-Naula, and L. Azpilicueta, "Comparative Study of Artificial Neural Network Based Channel Equalization Methods for mmWave Communications," *IEEE Access*, vol. 9, pp. 41678–41687, 2021.
[65] M. Kottkamp, A. Pandey, A. Roessler, R. Stuhlfauth, and D. Raddino, *5G New Radio - Fundamentals, Procedures, Testing Aspects*. Munich, Germany: Rohde & Schwarz, 2019.